

## 2D Impurity Flow Imaging on MAST with Coherence Imaging

S. A. Silburn<sup>1</sup>, R. M. Sharples<sup>1</sup>, C. A. Michael<sup>2</sup>, J.R. Harrison<sup>3</sup>, H. Meyer<sup>3</sup>, J. Howard<sup>2</sup>, K. Gibson<sup>4</sup>

<sup>1</sup>Durham University, Durham DH1 3LE, UK

<sup>2</sup> The Australian National University, Canberra ACT 0200, AU

<sup>3</sup> EURATOM/CCFE Fusion Association, Abingdon OX14 3DB, UK

<sup>4</sup> York University, York YO10 5DD, UK

**Introduction** Coherence imaging (CI) is an optical diagnostic technique using polarisation interferometry which can be used for 2D Doppler flow imaging of impurities in fusion plasmas[1]. Its fine spatial sampling over a wide field of view is well suited for studying complex scrape-off layer and divertor flows, and enables tomographic inversion of the line-integrated measurements to obtain flow profiles on a poloidal cross-section[2]. Such data have applications in studying impurity transport, exhaust and confinement and could help benchmark SOL & divertor modelling crucial to designing next generation fusion devices. A coherence imaging instrument has recently been installed on the Mega Amp Spherical Tokamak (MAST) for passive imaging of carbon and helium flows in the SOL & divertor.

**Diagnostic System** The Doppler coherence imaging technique uses 2-beam interferometry: plasma light is split into two equal amplitude parts, which are delayed relative to each other by a time  $\tau$  and then recombined at a detector. For a narrow spectral line or multiplet of rest wavelength  $\lambda_0$  at the input, the detected signal as a function of  $\tau$  is a sinusoidal fringe pattern, oscillating within an envelope given by the Fourier transform of the line shape[1]. Wavelength shifts of the input spectrum cause

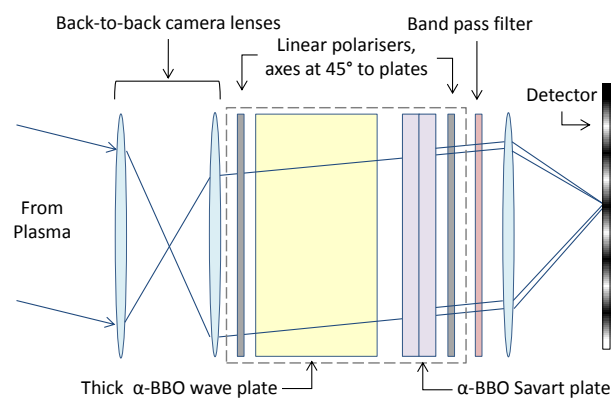


Figure 1: Schematic of the diagnostic optical design. The dashed box indicates a temperature regulated mounting cell.

small changes in the sinusoidal fringe frequency, resulting in a phase shift in the fringes of  $\Delta\phi/\kappa\phi_0 = \Delta\lambda/\lambda$ , where  $\phi_0(\tau) = 2\pi\tau c/\lambda_0$  is the interferometer phase delay and  $\kappa$  corrects for any wavelength dispersion of the delay  $\tau$ . Doppler shifts of ion line emission can therefore be obtained by measuring phase shifts of the interferogram for a known value of  $\kappa\phi_0$ .

A schematic of the MAST CI optical system is shown in Fig. 1. Back-to-back f=17-70mm (zoom) and f = 105mm F-mount camera lenses produce an image of the plasma focused at in-

finity. The zoom function of the plasma facing lens allows adjustment of the diagnostic field of view from 9° - 40°. In the collimated beam after the two lenses is a linear polariser with its polarisation axis oriented vertically, followed by a high order  $\alpha$ -BBO waveplate with its fast axis at 45° to the polariser axis. This resolves the beam into equal amplitude, orthogonally polarised components and introduces a known delay, usually  $\kappa\phi_0 \approx 2000 \times 2\pi$  for the MAST system, between the two. An  $\alpha$ -BBO Savart plate (a type of polarising beamsplitter[3]) then produces a vertical displacement between the two beam components, resulting in an angle-dependent geometrical path difference and a set of horizontal fringes at the detector plane. A second polariser with its axis parallel to the first forces the two components to interfere at the detector. The birefringent plates and polarisers are mounted using a custom mounting system in a temperature stabilised cell, supplied by ANU. This temperature stabilisation reduces calibration drifts due to thermal expansion and thermo-optic effects in the  $\alpha$ -BBO components. The final image is formed by an  $f = 150$ mm F-Mount camera lens focused at infinity, onto which an interchangeable 50mm diameter, 3 cavity interference filter is fitted for spectral line selection. The impurity lines studied in MAST are C III (465nm), C II (514nm) and HeII (468nm). The detector used is a Photron APX-RS 10-bit CMOS camera, with 1024x1024  $17\mu\text{m}$  pixels and capable of frame rates of up to 3kHz at full resolution (up to 100kHz for smaller regions of interest).

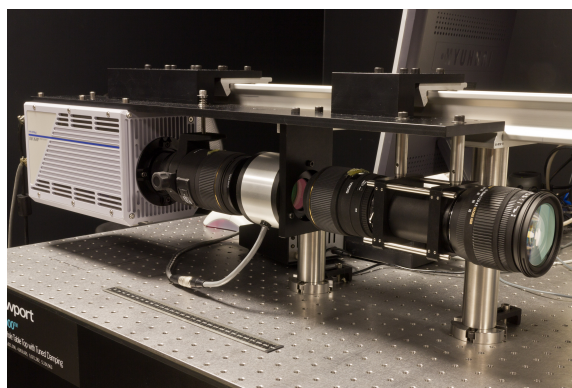


Figure 2: Photograph showing the construction of the MAST CI system (before installation on MAST), with a 30cm ruler for scale.

Figure 2: Photograph showing the construction of the MAST CI system (before installation on MAST), with a 30cm ruler for scale.

The image at the detector consists of a narrow band plasma emission image with horizontal fringes superimposed, which are used as a carrier signal to measure  $\Delta\phi$ . FFT based demodulation is used to recover the intensity and carrier phase at each image point. By subtracting a reference carrier phase image, a (line-of-sight integrated) Doppler shift measurement at each image point is obtained. For the MAST instrument the reference phase images are obtained, to within a DC offset, from flat fields illuminated with a Cadmium spectral lamp (this lamp has lines transmitted by both the He II and C III filters for our system).

The optical system is constructed on a custom aluminium base plate supported from a section of modified Newport X48 rail, which can be easily moved between different diagnostic ports (fig. 2). The maximum field of view corresponds to 1.4m x 1.4m of the poloidal cross-section with 1 - 2mm pixel pitch in the plasma. While the pixel scale and blurring of out-of-focus re-

gions determines the spatial resolution parallel to the fringes (usually horizontally), across the fringes (vertically) the spatial response is limited to approximately 1 fringe period, in this case 12 pixels.

**Initial Data** Data has been obtained for both mid-plane and divertor views with integration times of 1 - 20ms (depending on species and plasma conditions), and with flow resolution of approximately 1 - 4km/s. Measurements have included wide angle imaging covering both the high and low field side SOL, as illustrated in fig.3. Data has also been obtained for a radial midplane view covering the high field side SOL on both sides of the centre stack. Flow phenomena observed in these data include oppositely directed toroidal flows of C III and C II above and below the midplane during plasma startup, illustrated in fig. 4 (such behaviour is not seen in Helium). Interpretation and quantitative analysis of the flow phenomena seen in the initial data is now required.

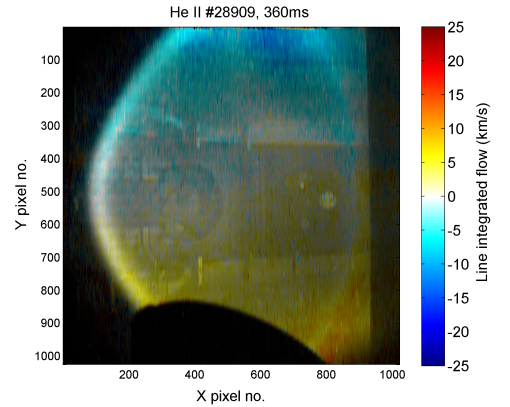


Figure 3: *Combined intensity and line integrated flow image for He II in a DND L-Mode NBI heated plasma (integration time 20ms) on a wide angle midplane view.*

startups, illustrated in fig. 4 (such behaviour is not seen in Helium). Interpretation and quantitative analysis of the flow phenomena seen in the initial data is now required.

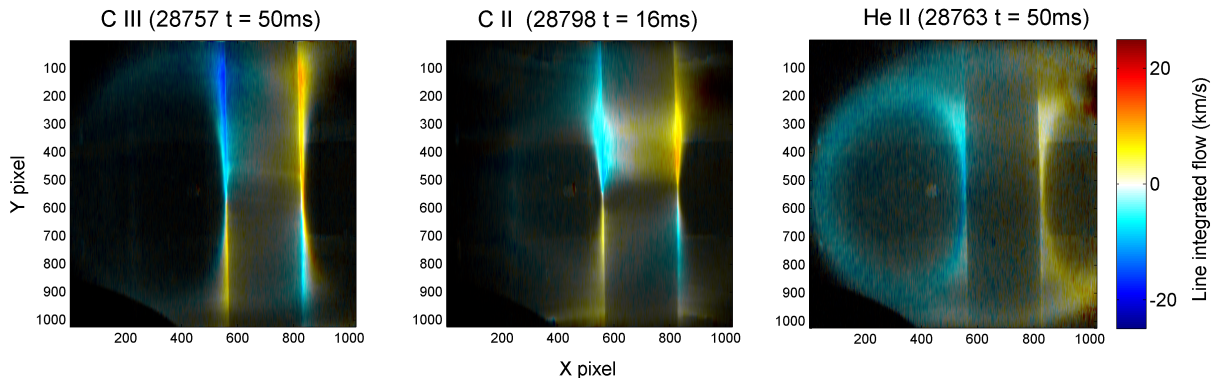


Figure 4: *Combination flow and intensity images for C III (left, integration time 2.5ms), C II (middle, integration time 16ms) and He II (right, integration time 16ms) early in the plasma shot. Flow reversal about the midplane is seen in C III and C II.*

In the divertor C III data has been obtained in NBI heated plasmas with time resolution up to 1ms. Oppositely directed toroidal flow projections are seen for the inboard and outboard divertor legs, which due to the helical magnetic field lines corresponds to flow on to both targets, as was observed with coherence imaging on DIII-D[2]. Fig.5 shows a combined intensity and line integrated flow image for C III in an NBI heated, H-Mode LSND plasma.

The large amount of information provided by CI enables tomographic reconstruction of

poloidal cross-sections of flows. Under assumptions of  $v_{||} \gg v_{\perp}$  and toroidal symmetry, this can be reduced to a scalar problem which can be solved with iterative reconstruction techniques[2]. A reconstruction code for the MAST system has been developed in MATLAB, and is now being tested and further developed using the initial divertor C III measurements. Fig.5 shows the best tomographic fit to the H-mode divertor data obtained using a simple simultaneous algebraic reconstruction technique (SART) implementation, and the corresponding poloidal flow and emissivity profile. Patterning is seen on the inner divertor leg in both the reconstruction and line integrated data, due to the plasma emissivity varying at spatial scales smaller than the carrier fringes on the image.

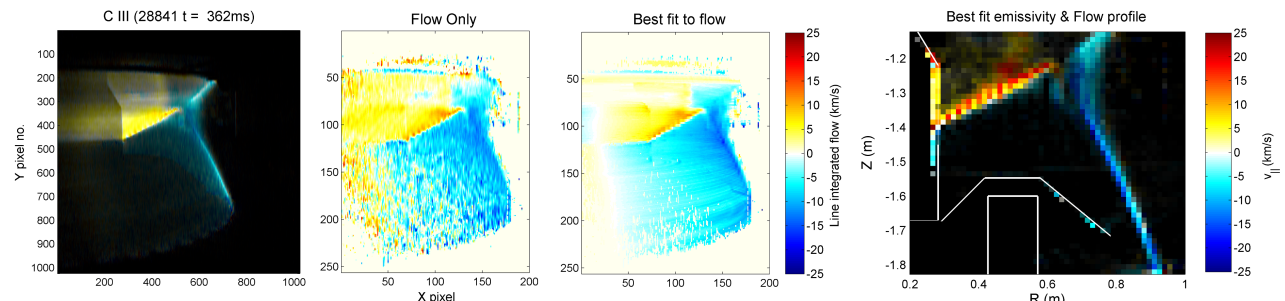


Figure 5: CIII divertor data, H-Mode LSND plasma and 2ms integration time. Left to right: combined intensity and flow image, flow only image, best tomographic fit to flow image, and tomographically reconstructed  $v_{||}$  and intensity image.

**Conclusions** Wide angle SOL and divertor imaging of intrinsic impurity flows on MAST has been demonstrated using coherence imaging. Data has been obtained with time resolution of 1 - 20ms and flow resolution of 1-4km/s. Features of the initial data include reversal of toroidal CII and CIII flows in the high field side SOL above and below the midplane during startup. Analysis of the observed flow behaviour is in progress. Lower divertor measurements show C III flowing towards the strike points, and tomographic inversion of divertor data has been developed and is being tested.

## References

- [1] J. Howard, J. Phys. B: At. Mol. Opt. Phys. **43**, 144010 (2010)
- [2] J. Howard, A. Diallo, M. Crease et al. Rev. Sci. Instrum. **81**(10), 10E528 (2010)
- [3] J. Li, J. Zhu, X. Hou, Opt. Commun. **284**(5), 1127 (2011)

This work was funded partly by the RCUK Energy Programme under grant EP/I501045 and the European Communities under the contract of Association between EURATOM and CCFE. The views and opinions expressed herein do not necessarily reflect those of the European Commission. SAS is funded by an EPSRC doctoral studentship. We thank Rutherford Appleton Laboratory for the loan of the Photron APX-RS camera.